

MULTIFRACTAL ANALYSIS OF $\text{CoFe}_2\text{O}_4/2\text{DBS}/\text{H}_2\text{O}$ FERROFLUID FROM TEM AND SANS MEASUREMENTS

CRISTINA STAN¹, MARIA BALASOIU^{2,3,*}, A. I. IVANKOV², C.P. CRISTESCU¹

¹“Politehnica” University of Bucharest, Department of Physics, Faculty of Applied Sciences,
Romania, E-mail: cstan@physics.pub.ro;

²Joint Institute for Nuclear Research, 141980, Dubna, Russia;

³“Horia Hulubei” National Institute of Physics and Engineering,
P.O. Box.MG-6, Bucharest, Romania,

*Corresponding author: balasoiumaria@yahoo.com

Received December 9, 2014

Abstract. In this paper we present preliminary investigations on the morphological properties and the multifractal characteristics of CoFe_2O_4 nanoparticles coated with a double layer of dodecylbenzenesulphonic acid and dispersed in double distilled water. We analyze TEM images and compute a multifractal spectrum that reveals universal multifractality. A comparison with fractal approach applied to SANS data is presented, and consistency of results is demonstrated.

Key words: CoFe_2O_4 nanoparticles, multifractal spectrum, SANS and TEM measurements.

1. INTRODUCTION

Natural objects do not have precise fractal dimensions as mathematically generated fractals but have a structure characterized by a fractal dimension which usually slightly varies with the observed scale. The irregularities described by the multifractal measures contain information about the process evolved in the generation process or about the local interactions that lead to spatial arrangement or aggregates formation. Multifractality has been reported in many systems, from biology to technology and from medicine to economy [1–4] including also magnetic fluids [5–10].

Transmission electron microscopy (TEM) and small-angle neutron scattering (SANS) are among the most useful technical approaches for extracting numerical data on ferrofluid complex structure of the magnetic fluids. The main characteristics of this type of colloidal suspension are to be polydisperse, containing different aggregates and micelles ([11–13]).

In this study, we present new properties of double distilled water based CoFe_2O_4 using the multifractal investigation of TEM images and SANS data.

2. TEM DATA AND MULTIFRACTAL ANALYSIS

Morphology and structure of $\text{CoFe}_2\text{O}_4/2\text{DBS}/\text{H}_2\text{O}$ ferrofluid is investigated using TEM measurements. TEM analysis was carried out on a LEO 912 AB OMEGA transmission electron microscope with an accelerating voltage of 120 kV (Advanced Technology Centre, Moscow). One droplet of water dispersion of CoFe_2O_4 nanoparticles was dropped on a carbon-coated copper grid and then dried naturally before recording the micrographs.

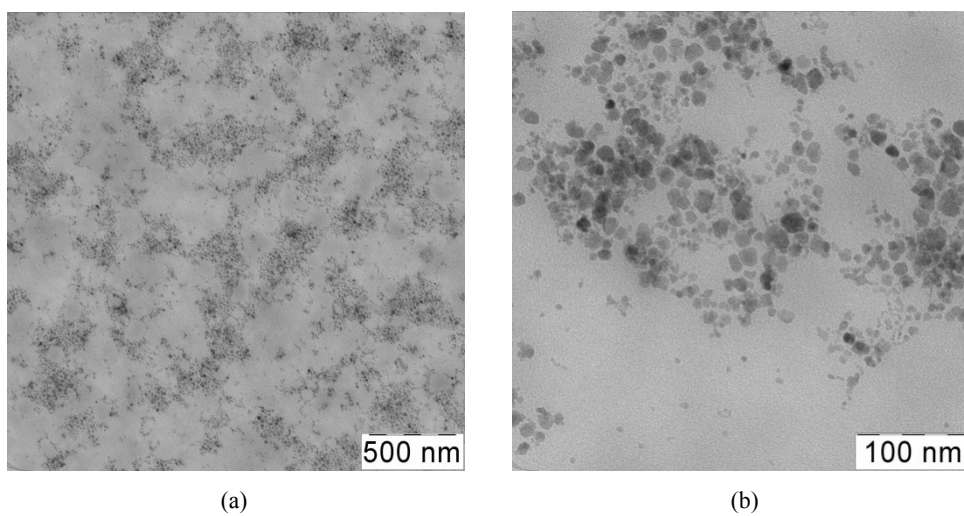


Fig. 1 – TEM images of CoFe_2O_4 nanoparticles coated with dodecylbenzene sulphonic acid dispersed in water with two different resolutions as shown on each image.

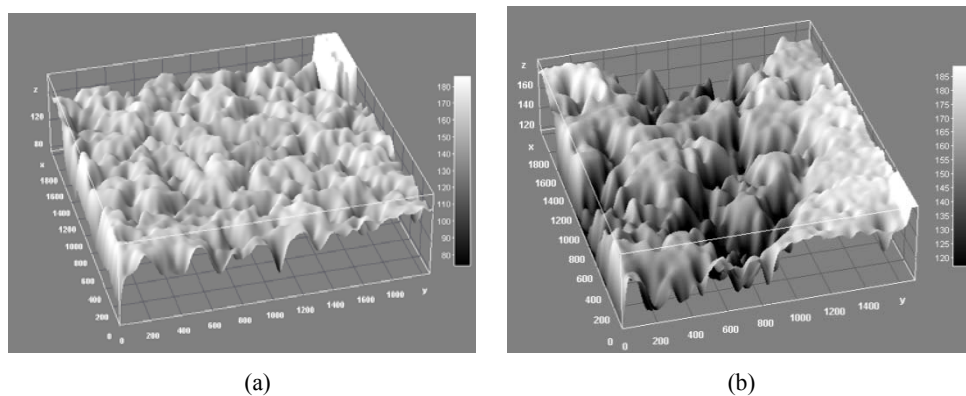


Fig. 2 – 3D image reconstruction in arbitrary units corresponding to the fragments of TEM images from Fig. 1a – left and Fig. 1b – right.

TEM images show a rather non-uniform spatial distribution of particles with specific preferred arrangements in “cluster-like” conglomerates (Fig. 1). Using the 3D reconstruction with the algorithm presented in [14], a qualitative description of the morphology of particles and their spatial arrangement can be obtained (Fig. 2). In order to have improved resolution only fragments of the TEM images from Fig. 1 were processed. The 3D images allow the estimation on the size and shape of the particle conglomerates, at least qualitatively. The representations in Fig. 2 show, in arbitrary units, the relative dimension of the spatial arrangement of the ferrofluid particles.

The concept of multifractality refers to the fact that different sections of the data are characterized by different values of the fractal dimension. A usual way of describing fractal properties is by computation of the multifractal spectrum $f(\alpha)$ from the partition function exponent $\tau(q)$ *versus* the generalized moment q , using the Legendre transform [15]

$$f(\alpha) = q\alpha - \tau(q) \quad (1)$$

and

$$d\tau(q)/dq = \alpha. \quad (2)$$

The generalized dimensions are defined by the relationship:

$$D(q) = \frac{\tau(q)}{q-1}. \quad (3)$$

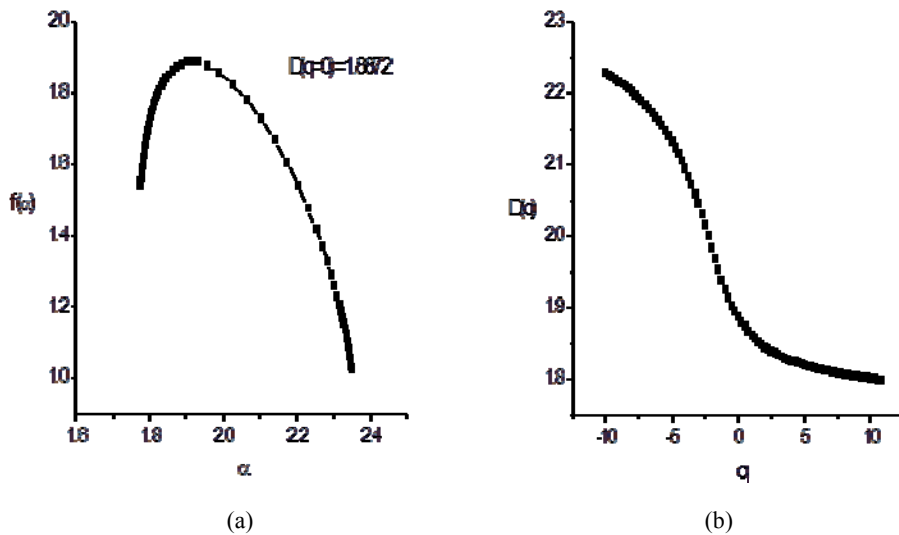


Fig. 3 – Multifractal spectra (a) and the generalized dimension for the TEM image (b) from Fig. 1a.

The multifractal spectra based on the partition function exponent computed using the box-counting method proposed and developed by Chhabra and Jensen [16] are shown in Fig. 4.

Figure 3 shows the multifractal spectra and the generalized dimension for the TEM images from Fig. 1a. The result is an average of computation carried out on four different zones of the TEM images. The meaning of the analysis given in Fig. 4 is directly related to the physical features of magnetic cores co-precipitation process as well as to the non-magnetic shell formation during the nanoparticle stabilization in deionized water considering the balance between the magnetic dipole attractions and electrostatic repulsions within the magnetic fluid volume [5, 6].

Muzy *et al.* [17] considered that the exponent of the partition function procedure, under some restrictions on the allowed values of q , can be related to the structure function exponent $\zeta(q)$. For multifractal processes, the exponent $\zeta(q) = \tau(q) + 1$ is nonlinear and concave, and can serve to the definition of a function $K(q)$ [18] as:

$$K(q) = qH - \zeta(q), \quad (4)$$

where

$$H = \zeta(1) = \tau(1) + 1. \quad (5)$$

Equation (4) shows that $K(q)$ represents a correction given by the function $\zeta(q)$ from linearity (characteristic of monofractal series). As a measure of inhomogeneity it can be defined the intermittency parameter:

$$C_1 = C(1) = \left. \frac{dK}{dq} \right|_{q=1}, \quad (6)$$

with values in the range between $C_1 = 0$, for a homogeneous space-filling process and $C_1 = d$, where d is the dimension of the space supporting the process ($d = 2$ for the present situation). Very low C_1 , close to zero, characterize fields with values in the neighborhood of the mean almost everywhere, while large C_1 corresponds to fields with low values almost everywhere except in isolated locations where, the values are much higher than the mean [19].

The dynamics of a large class of physical, biological, geological and financial time series are demonstrated to be well approximated as universal multifractals [20–22]. We show that the spatial arrangement of ferromagnetic nanoparticles sequence satisfies the universal multifractal conditions reasonably well. The adopted procedure is similar with those presented in [22]: the $K(q)$ dependence is obtained from equations (4–5) using the values of $\tau(q)$ numerically computed from the multifractal spectrum, using (2).

The curves $K(q)$ are convex and satisfy the conditions $K(0)=K(1)=0$, $K(q)<0$, $q \in (0,1)$, $K(q)>0$, $q > 1$ as shown in Fig. 4.

According to the universal multifractal hypothesis [21], some multifractals possess the property of a complete description of the whole statistics of a given field with only three basic parameters H , C_1 and α_L (Lévy index). Under universal multifractal hypothesis, the scaling moment function is written as:

$$K(q) = \begin{cases} \frac{C_1}{\alpha_L - 1} (q^{\alpha_L} - q) & \alpha_L \neq 1 \\ C_1 q \ln q & \alpha_L = 1 \end{cases} \quad (7)$$

where C_1 is given by (6) and α_L is computed as $\alpha_L = 1 - K'(1)/K'(0)$.

In the case of the universal multifractals, the function $K(q)$ defined by (4) is identical to $K(q)$ defined by (7) for $\alpha_L \neq 1$ and the values of the parameters C_1 and α_L , computed using the scaling moment function in the respective formulas give similar results.

The very good fitting of the dependence $K(q)$ (Fig. 4) as α_L -order polynomial (parabolic) demonstrates both that the investigated structure is an universal multifractal and that the diameter distribution is close to lognormal. This is a further confirmation that the log-normal distribution is the most adequate in analyzing the polydispersity. Accordingly, the physical mechanism of cluster formation is governed by the law of proportionate effects [23] that could be mainly responsible for ferrophase diameter distributions.

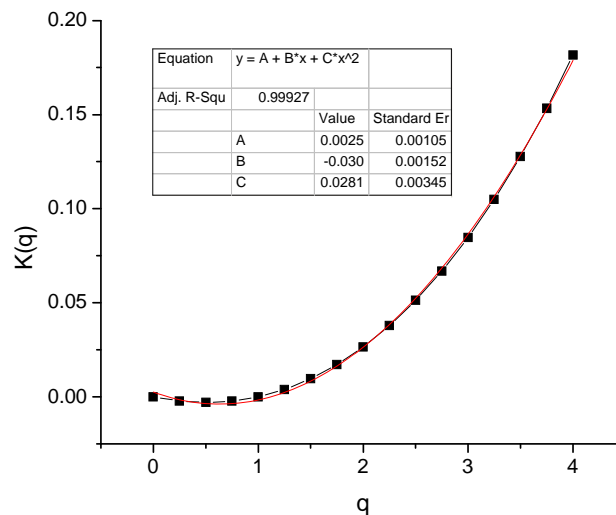


Fig. 4 – Testing the multifractality and finding the parameters in the universal multifractal hypothesis ($K'(0) = -0.031$; $K'(1) = 0.028$).

3. COMPARISON WITH SANS DATA

Small angle neutron scattering (SANS) experiments were performed at the time-of-flight YuMO spectrometer [24, 25] in function at the high flux pulse IBR-2 reactor, JINR Dubna. The experiments were carried out at a sample-to-detector distances of 5.28 m and 13.04 m, resulting in a Q range of $(0.007 \div 0.3) \text{ \AA}^{-1}$. The sample diameter and thickness in the beam were 14 mm and respectively 1 mm. The measured neutron scattering spectra were corrected for the transmission and the thickness of the sample, background scattering on the experimental cuvette and on vanadium reference sample using the SAS software, providing the neutron scattering intensity.

Fractal SANS scattering intensity curves usually present three regions that can be approximated as linear curves, corresponding to power law dependences with different exponents $I(Q) = I_0 Q^\beta$. In the case of the curve shown in Fig.5, the linear fit is only shown for the median region which is of interest for the present study. This zone extends for a relatively large range of the scattering vector Q , indicating a fractal nature of the ferrofluid sample. The slope of the linear part of the curve is $\beta = 3.81 \pm 0.07$ demonstrating that the scattering objects are in a first order approximation surface fractals ($\beta > 3$) with main fractal dimensions $D_s = 6 - \beta = 2.19$. This value is specific to highly branched surface fractals [10].

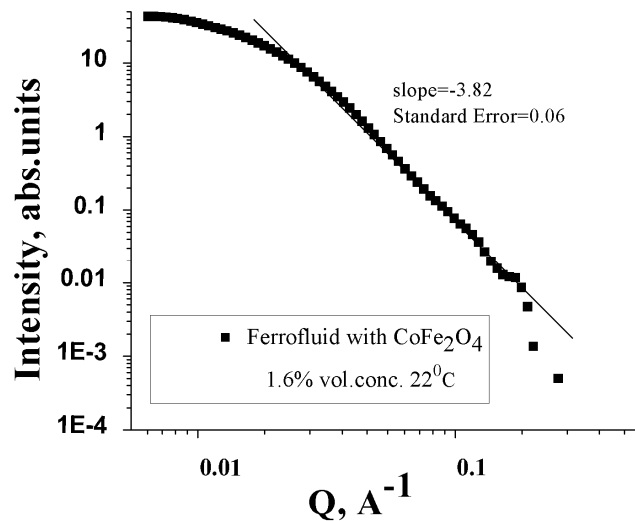


Fig. 5 – Experimental (points) and fitted line for scattering curve SANS for CoFe_2O_4 nanoparticles coated with dodecylbenzene sulphonic acid dispersed in water (1.6%) measured at 22°C .

As visible from Fig. 3b, this dimension can be found in the plot of the generalized dimension corresponding to $q = -7$ and in the multifractal spectrum computed from TEM images (Fig. 3a).

In the spectrum of the generalized dimensions, for $q < 0$, the highest contribution to $D(q)$ comes from the least visited cells [24] or from small fluctuations from the mean. In this context, as expected, SANS power law dependence in the monofractal approximation for the considered linear region gives mainly the contribution of the scattering process on small particle.

4. CONCLUSION

In this paper we analyze experimental data from TEM and SANS measurements of CoFe_2O_4 nanoparticles coated with a double layer of dodecylbenzene sulphonic acid and dispersed in double distilled water. We show that, at least qualitatively, the morphology of the magnetic particles, the relative dimensions and spatial arrangement is reflected in the 3D reconstruction of TEM image. The multifractal analysis of the TEM image shows that the investigated system is characterized by a set of fractal dimensions, reflected in the multifractal spectrum and in a set of the generalized dimensions. Using different methods of computation (box-counting and structure function formalism), we demonstrate that this system can be considered as universal multifractal.

The good fitting with a parabola of the function describing the departure from the monofractality ($K(q)$) demonstrates that the particle distribution described by TEM image is close to lognormal. The result is a further confirmation that the log-normal distribution is the most adequate in describing the system polydispersity. Comparison with the fractal approach, demonstrate acceptable agreement. The fractal dimension obtained from analysis of SANS data can be found in the multifractality spectrum and corresponds to q -order moment function for small fluctuations.

Further investigation are under progress for analyzing the SANS curves for other nanoparticulate systems using multifractal methods.

Acknowledgements. The authors acknowledge the financial support of UPB-JINR Cooperation Scientific Projects No.96/17.02.2014 item 44 and No.95/17.02.2014 item 38. M.B. acknowledges S.S. Abramchuk (Advanced Technologies Center, Moscow) for the TEM images.

REFERENCES

1. O. Pont, A. Turiel, C. J. Pérez-Vicente, *Phys. A: Stat. Mech. Appl.* **388**, 2025–2035 (2009).
2. S. Lovejoy, W. J. S. Curri, Y. Tessier, M. R. Claereboudt, E. Bourget, J. C. Roff, E. Schertzer, *J. Plankt. Res.* **23**, 117–141 (2001).
3. E.I. Scarlat, C. Stan, C. P. Cristescu, *Physica A: Stat. Mech. Appl.* **379**, 188–198 (2007).
4. C. Stan, C.P. Cristescu, D.G. Dimitriu, *Rom. J. Phys.* **56**, 79–82 (2011).
5. C. Stan, D. E. Creanga, C. P. Cristescu, M. Racuciu, *Bull. Inst. Pol. Iasi, Tom LVI (LX)* **4**, 153–158 (2010).

6. C. Stan, C.P. Cristescu, M. Balasoiu, Int. Conf. *Condensed Matter Research at the IBR-2*, Dubna, 2014, Book of abstracts, p. 53.
7. M. Hirabayashi, Y. Chen and H. Ohashi, *J. Magn. Magn. Mater.* **252**, 138–140 (2002).
8. E. Elfimova, *Magnetohydrodynamics* **40**, 43–52 (2004).
9. I. Takahashi, N. Tanaka and S. Doi, *J. Appl. Cryst.* **36**, 244–248 (2003).
10. A. Y. Cherny, E. M. Anitas, A. I. Kuklin, M. Balasoiu and V. A. Osipov, *J. Appl. Cryst.* **43**, 790–797 (2010).
11. M. Balasoiu, A.I. Kuklin, B. Grabcev, D. Bica, *Rom. Rep. Phys.* **49**, 379–384 (1998).
12. M. Balasoiu, M.V. Avdeev, A.I. Kuklin, V.L. Aksenov, D. Bica, L. Vekas, D. Hasegan, Gy. Torok, L. Rosta, V.M. Garamus, J. Kohlbrecher, *Magnetohydrodynamics* **40**, 359 (2004).
13. M. Balasoiu, M.V. Avdeev, V.L. Aksenov, V. Ghenescu, M. Ghenescu, G.Y. Torok, L. Rosta, D. Bica, L. Vekas, D. Hasegan, *Rom. Rep. Phys.* **56**, 601–607 (2004).
14. M.D. Abramoff, P.J. Magalhaes, S.J., Ram, *Biophot. Int.* **11**, 36–42 (2004).
15. R. C. Hilborn, *Chaos and Nonlinear Dynamics*, Oxford Univ. Press, 1994.
16. A. Chhabra, R.V. Jensen, *Phys. Rev. Lett.* **62**, 1327–43 (1989).
17. J. F. Muzy, E. Bacry, A. Arneodo, *Phys. Rev. E* **47**, 875 (1993).
18. F. Schmitt, S. Lovejoy, D. Schertzer, *Geophys. Res. Lett.* **22**, 1689 (1995).
19. E. Paux E, P. Sourdille, J. Salse *et al.*, *Science* **322**, 101 (2008).
20. Y. Tessier, S. Lovejoy, P. Hubert, D. Schertzer, and S. Pecknold, *J. Geophys. Res.* **31D**, 427 (1996).
21. L. Seuront, F. Schmitt, Y. Lagadeuc, D. Schertzer, and S. Lovejoy, *J. Plankt. Res.* **21**, 877 (1999).
22. C. Stan, M.T. Cristescu, L. Iarinca-Buimaga, C.P. Cristescu, *J. Theor. Biol.* **321**, 54–62 (2013).
23. J. Eeckhout, *American Economic Review* **94**, 1429–1451 (2004).
24. A.I. Kuklin, A.Kh. Islamov, and V.I. Gordely, *Neutron News* **16**(3), 16 (2005).
25. A.I. Kuklin, A.Kh. Islamov, Yu.S. Kovalev, P.K. Utrobin, and V.I. Gordely, *J. Surf. Invest. X-Ray, Synchr., Neutron Tech.* **6**, 74 (2006).
26. C.P. Cristescu, *Dinamici neliniare și haos*, Edit. Academiei Române, 2009.